pubs.acs.org/Biomac

Article

Phase-Separated Multienzyme Biosynthesis

Miao Liu, Sicong He, Lixin Cheng, Jianan Qu, and Jiang Xia*

Cite This: *Biomacromolecules* 2020, 21, 2391−2399

Read Online

ACCESS | Metrics & More | Article Recommendations | Supporting Information

ABSTRACT: Liquid−liquid phase separation forms condensates that feature a highly concentrated liquid phase, a defined yet dynamic boundary, and dynamic exchange at and across the boundary. Phase transition drives the formation of dynamic multienzyme complexes in cells, for example, the purinosome, which forms subcellular macrobodies responsible for *de novo* purine biosynthesis. Here, we construct synthetic versions of multienzyme biosynthetic systems by assembling enzymes in protein condensates. A synthetic protein phase separation system using component proteins from postsynaptic density in neuronal synapses, GKAP, Shank, and Homer provides the scaffold for assembly. Three sets of guest proteins: a pair of fluorescent proteins (CFP and YFP), three sequential enzymes in menaquinone biosynthesis pathway (MenF, MenD, and MenH), and two enzymes in terpene biosynthesis pathway (Idi and IspA) are assembled via peptide−peptide interactions in the condensate. First, we discover that coassembly of CFP and YFP exhibited a broad distribution of the FRET signal within the condensate. Second, a spontaneous enrichment of the rate-limiting enzyme MenD in the condensate is sufficient to increase the 2-succinyl-6-hydroxy-2,4-cyclohexadiene-1-carboxylate production rate by 70%. Third, coassembly of both Idi and IspA in the protein condensate increases the farnesyl pyrophosphate production rate by more than 50%. Altogether, we show here that phase separation significantly accelerates the efficiency of multienzyme biocatalysis.

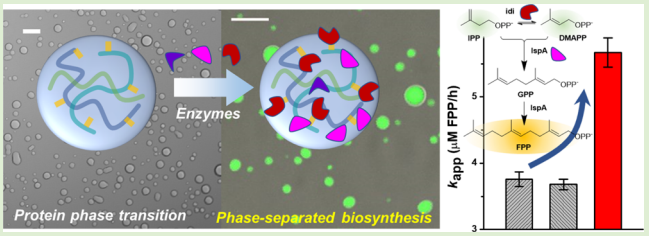

INTRODUCTION

How nature achieved an accelerated molecular conversion rates, when the catalysts—first nucleic acids, later proteinaceous enzymes—were still primitive remains enigmatic. One possibility is that physical interactions and processes, such as liquid−liquid phase separations (LLPS), helped to increase the catalytic efficiency.[1−3] Phase separation is prevalent in cells in the modern world now. We now know that some biomacromolecules spontaneously condense and form self-assembled liquid condensates, a.k.a. membraneless organelles, which serve as microcompartments to selectively concentrate certain molecules while excluding others.[4−8] The liquid condensates are highly mobile and dynamic: they can move around, fuse together, and exchange materials with the surrounding environment. Membrane-less organelles have participated in various cellular functions, such as gene transcription,[9] heterochromatin formation,[10,11] spindle apparatus assembly,[12] asymmetric cell division,[13] autophagy,[14,15] innate immune response,[16] and others.

How LLPS impacts cascade biocatalysis has been an appealing question to chemists. Metabolic enzymes can form condensates in bacteria, yeast, and mammalian cells, particularly under starvation or other stressful conditions.[17,18] Well characterized examples include cytidine triphosphate synthesis and purinosome.[19,20] Concentrating enzymes and substrates in phase-separated condensates segregates the biosynthetic pathway from others in the complex metabolic network[21] or substrate-channeling effect will lead to the marked rate increase of the cascade reaction and expedite metabolic flux inside phase-separated condensates.[22] This was first proved in synthetic polymer condensates.[23] For example, a hammerhead ribozyme showed up to 70-fold activity increase when concentrated along with its substrate RNA into phase-separated condensates made of synthetic polymers.[24] Notwithstanding, the synthetic polymer condensates are different from natural protein condensates, and the polymers cannot express inside cells. The interface between enzymes and protein phase-separated condensates better mimics the natural dynamic multienzyme complexes, such as the purinosome. Zhao et al. reported a light-based control of phase separation to give synthetic organelles in the metabolic pathway.[21]

Notwithstanding, previous strategies rely on direct fusion of phase-forming scaffold proteins with the guest proteins,[21,25] which however may affect the phase-forming property of the scaffold protein or decrease the enzymatic property. Interaction-driven assembly, instead, is a more efficient and general method to incorporate guest proteins into phase-separated condensates.[26,27] We, therefore, reason that an interaction-driven self-assembly will be a feasible method to construct

Received: March 3, 2020
Revised: April 20, 2020
Published: April 28, 2020

https://dx.doi.org/10.1021/acs.biomac.0c00321
Biomacromolecules 2020, 21, 2391−2399

phase-separated multienzyme catalytic systems. Here, we utilize a high-affinity peptide−peptide interacting pair. RIDD and RIAD are two peptide motifs derived from the natural proteins, cAMP-dependent protein kinase and the A kinase-anchoring proteins, respectively.[28−30] The 50-residue long RIDD motif (residual 12−61 of RIα) forms a stable dimer, and the dimer binds with an 18-residue peptide RIAD with a K_d of 1.0 nM.[31] Through the high-affinity peptide interactions, we assemble biosynthetic enzymes to a three-component phase separation system from postsynaptic density (PSD) in neurological synapses, including GKAP, Shank, and Homer, which are most abundant proteins in PSD and can self-assemble to form protein droplets both *in vivo* and *in vitro*.[32−35] Altogether, we assemble enzymes in the PSD-derived phase-separated protein condensates via peptide interactions and compare the overall biosynthetic efficiency in the presence or absence of phase-separated condensate.

MATERIALS AND METHODS

Phase Separation, Imaging, and Centrifugation Assay. All proteins were prepared in buffer containing 50 mM Tris, pH 8.0, 100 mM NaCl, and 1 mM EDTA. After high-speed centrifugation to remove any protein aggregates, proteins were then mixed together with the same buffer at designated concentration to form phase separation. For microscopic imaging, protein mixtures were injected into a homemade flow chamber comprised of a glass slide sandwiched by a coverslip with one layer of double-sided tape as a spacer. Differential interference contrast and fluorescent images were captured using a Nikon D-Eclipse C1 Confocal Microscope, Nikon C2+ confocal microscope, or Leica SP8 confocal microscope at room temperature. The fluorescence intensities were analyzed by ImageJ software. The centrifugation/sodium dodecyl sulfate−polyacrylamide gel electrophoresis (SDS−PAGE) assay was carried out as the following. After mixing the proteins for 20 min at room temperature, the mixture was centrifuged at 16,000*g* for 10 min at 20 °C. Then, the supernatant was removed and stored for PAGE analysis, and the pellet was resuspended in buffer to the same volume for PAGE analysis. Proteins from both S and P fractions were analyzed by SDS−PAGE with Coomassie blue staining. The pellet percentage was calculated by analyzing the band intensities of S and P fractions using ImageJ software.

Fluorescence Lifetime Imaging Microscopy-Based Fluorescence Resonance Energy Transfer Assay. Fluorescence resonance energy transfer (FRET) measurement was performed on a home-built two-photon fluorescence lifetime imaging microscope at room temperature. The cyan fluorescent protein (CFP) fluorescence was excited by an 810 nm femtosecond laser, and its lifetime was recorded by a time-correlated single photon-counting module at 481 nm. The CFP lifetime was calculated by bi-exponential curve fitting. The average lifetime was calculated by lifetime curve fitting on the average of all pixels.

Standard deviation (SD) is used to quantify the amount of variation of fluorescence lifetimes of a particle, which is defined as

$$\mathrm{SD} = \sqrt[2]{\frac{\sum_{i=1}^{n}(x_i - \mathrm{avg}(x))^2}{n-1}}$$

where n is the number of intensities, and $\mathrm{avg}(x)$ is the mean intensity of a particle. A low SD indicates that all the intensities are close to the mean of the particle while a high SD indicates that the intensities are spread in a wide range.

Participate coefficient (PC)[36−38] measures how diversely the fluorescence lifetimes of a particle are distributed among the intensity bins, that is, from 2300 to 4300, step by 500. It is defined as

$$\mathrm{PC} = 1 - \sum_{i=1}^{n}\left(\frac{w_i}{W}\right)^2$$

where n is the number of bins, W is the total number of pixels, and w_i is the number of pixels in bin i. PC ranges from 0 to 1. It is close to 1, when the intensities of a particle tend to be uniformly distributed among all intensity bins, and it approaches 0, if all intensities are in one single bin.

Cy5 Protein Labeling. The protein of choice was dissolved in 0.1 M sodium bicarbonate buffer, pH 8.3 at a concentration of ∼5 mg/mL. Sulfo-Cy5 NHS ester dissolved in dimethyl sulfoxide was slowly added under stirring. The molar ratio of protein to Cy5 was 1:1. After incubating for 1 h at room temperature, reaction was terminated by 200 mM Tris, pH 8.3. Cy5-labeled proteins were separated on the HiTrap Desalting column. Protein concentration and labeling efficiency were determined by absorbance of 280 and 650 nm.

Enzymatic Assay of Menaquinone Biosynthetic Enzymes. The reaction solution includes 100 μM chorismate, 2 μM MenF, 1 μM MenD, 1.5 mM Mg^{2+}, 1 mM 2-ketoglutarate, 10 μM ThDP, and 20 nM MenH-RIDD and was incubated together in a buffer containing 50 mM Tris, pH 7.6, 100 mM NaCl, and 1 mM DTT at room temperature. For enzyme reaction in the presence of the phase condensates, 5 μM each of GKAP, Homer (with or without RIAD), and Shank (with or without RIAD) was added. Before reaction starts, all the components except for chorismate were mixed together for 10 min to form the phase condensates. For control reactions in the absence of the phase condensate, the same volume of storage buffer was added. Then, chorismate was added to initiate the reaction. Reaction was terminated by 0.1% trifluoroacetic acid and quantified by high-performance liquid chromatography. The apparent reaction rates (k_{app}) were deduced by linear curve fitting of 2-succinyl-6-hydroxy-2,4-cyclohexadiene-1-carboxylate (SHCHC) concentration increase within the first 10 min.

Enzymatic Assay of Terpene Biosynthetic Enzymes. The reaction solution includes 67 μM isopentenyl pyrophosphate (IPP), 0.5 μM idi-RIDD, 1 μM RIDD-IspA, and 2 mM Mg^{2+} and was incubated in a buffer containing 50 mM Tris, pH 7.6, 100 mM NaCl, and 1 mM DTT at room temperature. For enzyme reaction in the presence of the phase condensates, 5 μM each of GKAP, Homer (with or without RIAD), and Shank (with or without RIAD) was added. Before reaction starts, all the components except for IPP were mixed together for 10 min to form the phase condensate. For control reactions in the absence of the phase condensate, the same volume of storage buffer was added. Then, IPP was added to initiate the reaction. Reaction was terminated by 0.01% triethanolamine, and the final product, farnesyl pyrophosphate (FPP), was analyzed by liquid chromatography−mass spectrometry. The apparent reaction rates (k_{app}) were deduced by the linear curve fitting of FPP concentration increase within the first hour.

RESULTS AND DISCUSSION

Engineering a Phase Separation System. First, we show that the interacting peptide RIAD can be fused to phase-forming scaffold proteins, Shank and Homer, and the RIAD tag does not significantly affect the phase formation property. The GKAP, we use, includes the sequences of PSD-95 GK-binding repeats and a C-terminal extended PDZ-binding motif. Shank is from Shank3 protein including an N-terminal extended PDZ domain, a Homer-binding sequence and a Cortactin-binding sequence in the poly proline region, followed by a C-terminal SAM domain, mediating self-oligomerization, and a GB1 tag was added at the N-terminus to increase the solubility of Shank construct.[39] The 18-residue RIAD peptide was fused at the N-terminus of Homer to give RIAD-Homer or inserted between the GB1 tag and Shank to give RIAD-Shank (Figure 1A). All five proteins were successfully constructed, expressed, and purified. Mixing GKAP/Shank/Homer or GKAP/RIAD-Shank/RIAD-Homer resulted in turbid solutions with condensates observable under optical microscopy (Figure 1B), indicating the formation of LLPS. Protein phase

https://dx.doi.org/10.1021/acs.biomac.0c00321
Biomacromolecules 2020, 21, 2391−2399

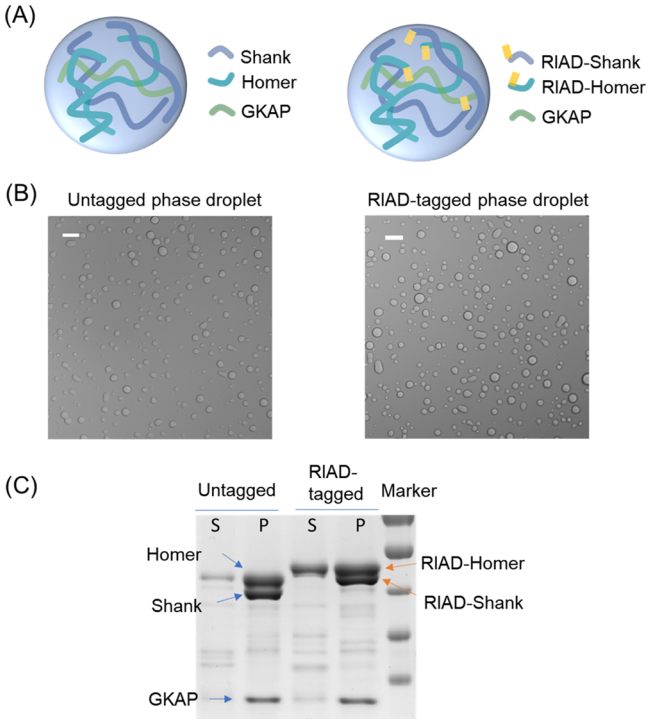

Figure 1. RIAD-tagged phase separation system based on PSD proteins. (A) Schematic comparison of the untagged phase separation system and the modified phase separation system with RIAD peptide tags. (B) Phase formation under a microscope by mixing untagged and RIAD tagged scaffold proteins at 5 μM. Scale bar: 10 μm. (C) SDS−PAGE analysis from the centrifugation assay showing the distribution of phase scaffolds between diluted phase/supernatant (S) and condensed phase/pellet (P) at 5 μM.

condensates can be precipitated by ultracentrifugation of the solution. The supernatant/diluted phase (S phase) and the precipitate/condensed phase (P phase) were then analyzed by SDS−PAGE. The majority of the scaffold proteins was found in the P phase, indicating successful formation of the protein phase separation (Figure 1C). This result shows that fusing the RIAD peptide with phase-forming scaffold proteins does not pose adverse effect on phase formation.

Fluorescent Protein in the Protein Condensate. We next assembled a fluorescent protein EGFP−RIDD (RIDD motif fused at C-terminus of EGFP) with the protein condensates through the RIDD−RIAD interaction. RIAD-Homer and RIAD-Shank and GKAP at 5 μM can efficiently incorporate and condense EGFP−RIDD within the protein condensates (Figure 2B). The fluorescent signal of EGFP inside the condensate was 50-fold higher than surrounding solution. Although without RIDD or RIAD tag, EGFP was only modestly enriched in the condensates (only fourfold higher without RIDD and twofold higher without RIAD). This, then, represents a "low-level" spontaneous absorption of external guest proteins through nonspecific protein interactions. For up to 4 μM EGFP−RIDD, more than 50% of the guest protein resided in the P phase without compromising the phase formation (Figures 2C and S1A). Confocal microscopic images also clearly indicated the enrichment of EGFP−RIDD in protein condensates (Figure S1B). Fluorescence recovery after photobleaching indicated that the incorporated EGFP−RIDD protein maintained its mobility with the condensates, despite a low recovery rate (Figure S1C). These results indicate that the guest protein EGFP can be incorporated into phase-separated protein condensates through peptide−peptide interaction, without altering the integrity of phase formation.

Assembly of a Pair of Fluorescent Proteins in the Condensate. We, then, examined the simultaneous assembly

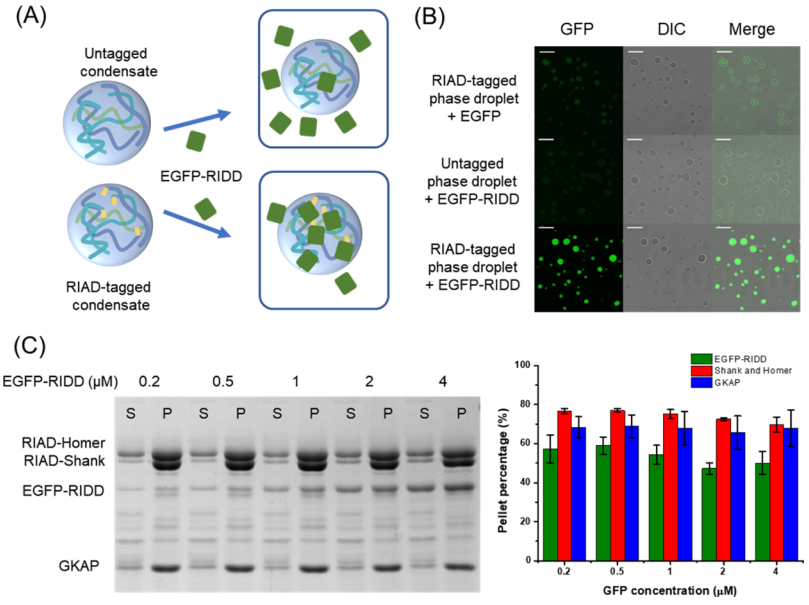

Figure 2. Assembly of fluorescent protein EGFP-RIDD into protein condensates. (A) Schematic design of the protein assembly system. Untagged system using Shank and Homer to form phase separation, and the RIAD-tagged system using RIAD-Shank and RIAD-Homer to form phase separation. (B) Confocal images showing EGFP−RIDD was significantly concentrated in the protein phase with the help of RIAD−RIDD interaction. Scale bar: 10 μm. Protein scaffolds 5 μM and EGFP 0.1 μM. (C) SDS−PAGE analysis showing the distribution of phase scaffolds and EGFP−RIDD between diluted phase/supernatant (S) and condensed phase/pellet (P) at indicated concentration. Protein scaffold concentration was set at 5 μM.

https://dx.doi.org/10.1021/acs.biomac.0c00321
Biomacromolecules 2020, 21, 2391−2399

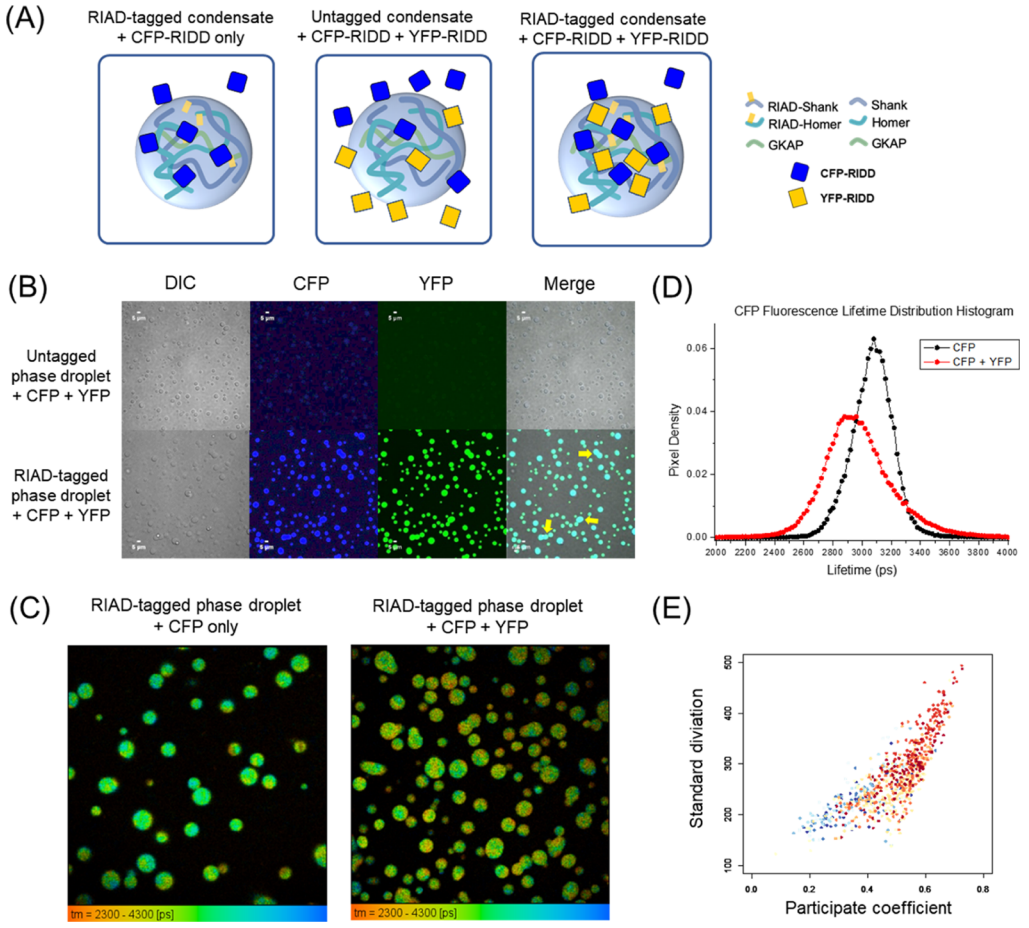

Figure 3. Assembly of CFP and YFP within the protein condensate. (A) Schematic illustration of three systems. (B) Confocal images of CYP, YFP, and merge channel showing that CFP−RIDD and YFP−RIDD can be recruited in one condensate. Scale bar: 5 μm. Protein scaffolds 5 μM, CFP−RIDD, and YFP−RIDD 0.1 μM. Yellow arrows point to droplets that in the fusion process. (C) Representative fluorescence lifetime images showing the CFP lifetime in the condensate. CFP only: condensate with CFP−RIDD only; CFP + YFP: condensate with CFP−RIDD and 20 times of YFP−RIDD. Color coding was continuous from 2000 to 4000 ps. Protein scaffolds 5 μM, CFP−RIDD 0.1 μM, and YFP−RIDD 2 μM. (D) Lifetime distribution histogram obtained by counting CFP lifetime of all the pixels in lifetime images. (E) Scatter plot showing the SD and PC of CFP lifetime in every single particle. Cold colors correspond to the condensates in CFP images while warm colors correspond to the condensates in CFP + YFP images.

of two fluorescent proteins in the condensates by peptide interaction. We fused the RIDD domain to the C-terminus of a CFP and a yellow fluorescent protein (YFP) to give CFP−RIDD and YFP−RIDD.[40,41] When both CFP−RIDD and YFP−RIDD at 100 nM were mixed with the three RIAD-tagged scaffold components at 5 μM, the CFP and YFP signals can be found to colocalize in the protein condensate, as shown in the confocal images (Figure 3B), indicating that the protein condensate can accommodate multiple fluorescent proteins driven by RIAD−RIDD interaction. There were some condensates undergoing the fusion process (yellow arrows in Figures 3B and S2A), showing the fluidity of the condensates. Further evidence is given by a lifetime-based FRET assay, which measures the fluorescence lifetime of the donor molecule (CFP−RIDD here). The fluorescence lifetime of the donor will decrease when it undergoes FRET with an acceptor molecule (YFP−RIDD here). Under a fluorescence lifetime imaging microscope (Figure 3C), the average fluorescence lifetime of CFP−RIDD in the protein phase was measured to be 3290 ps, which is comparable to the reported value in the literature.[40] When excess YFP−RIDD was added to the CFP-containing protein condensates, the lifetime of CFP decreased to 3070 ps, showing FRET effect between CFP−RIDD and YFP−RIDD. Interestingly, on the CFP lifetime heat map, an uneven distribution of the CFP lifetime was observed, indicating the heterogeneity of the condensate (Figure 3C). A statistical analysis of the distribution of CFP lifetime in each pixel indicated that, concomitant with the decrease of the overall lifetime of CFP−RIDD, the distribution of CFP lifetime became significantly wider (Figure 3D). Two measurements, SD and PC, were used to evaluate the fluorescence lifetime diversity. The CFP lifetime distributions in CFP only and CFP + YFP systems show distinct patterns (Figure 3E). As shown in the boxplots, the distributions of both SD and PC for the CFP + YFP figures are significantly higher than that of the CFP-only figures ($P < 2.2 \times 10^{-16}$, Mann−Whitney U test), indicating that the signals of CFP fluorescence lifetime are more diversely distributed in the CFP + YFP systems (Figure S2B). Altogether, the interaction-driven coassembly brought CFP and YFP into close proximity within a single condensate.

Menaquinone Biosynthetic Enzymes in the Protein Condensate. Next, we assembled enzymes that catalyze sequential reactions in menaquinone biosynthesis in the

https://dx.doi.org/10.1021/acs.biomac.0c00321
Biomacromolecules 2020, 21, 2391−2399

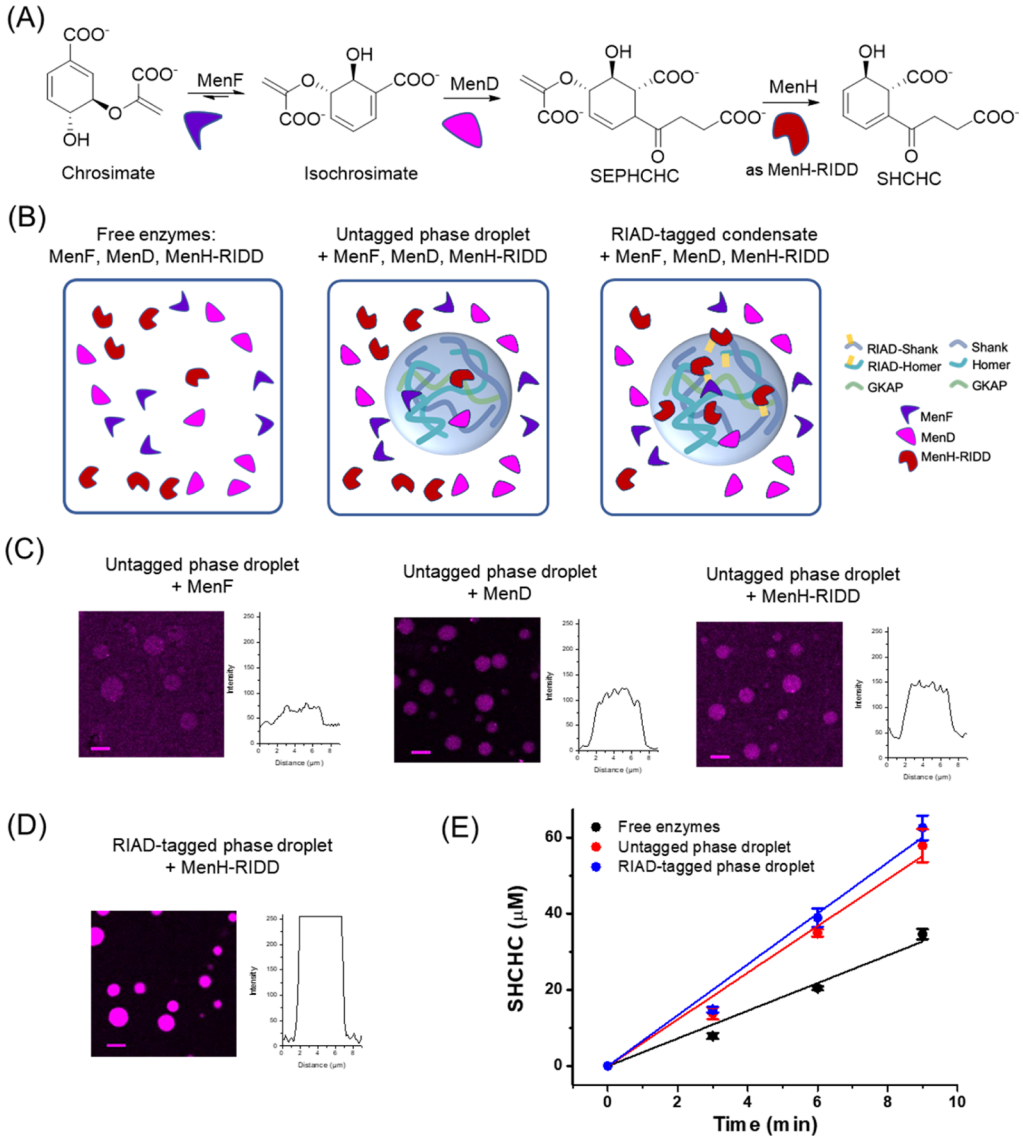

Figure 4. Assembly of menaquinone biosynthetic enzymes into protein condensate promotes cascade catalysis. (A) MenF, MenD, and MenH enzymes, and the reactions they catalyze. (B) Schematic illustration of the three catalytic multienzyme systems. (C) Confocal images showing enzymes were weakly concentrated in the untagged protein condensates, with quantification of Cy5 fluorescence intensities shown on the right. (D) Confocal image showing significant enrichment of MenH−RIDD in the RIAD-tagged protein condensates, with quantification of Cy5 fluorescence intensity of the condensate shown on the right. Scale bar: 5 μm. Protein scaffolds, 5 μM; enzymes, 1 μM with 5% labeled with Cy5. (E) Quantification of the initial rate of SHCHC production for comparison of the three systems.

protein condensate. The precursor of menaquinone (vitamin K2) SHCHC is synthesized from chorismate by a series of enzymes.[42,43] The first enzyme MenF converts chorismate to isochorismate through a rapid equilibrium,[44] followed by the addition of an α-ketoglutarate to generate 2-succinyl-5-enolpyruvyl-6-hydroxy-3-cyclohexadiene-1-carboxylate (SEPHCHC) by a thiamine diphosphate-dependent enzyme MenD,[45,46] and then elimination of a pyruvate catalyzed by MenH gives SHCHC (Figure 4A).[47] MenD is known to catalyze the rate-limiting step in the three-enzyme sequential reactions.[44−48] We have demonstrated that assembly of these three enzymes on quantum dots or using protein scaffolds can alter the cascade catalysis process.[30,48,49]

We next explored the formation of multienzyme catalytic system of MenF, MenD, and MenH. Expression vectors of MenF−RIDD, MenD−RIDD, and MenH−RIDD were constructed. MenF−RIDD, however, did not express as a soluble protein and was therefore not used in later experiments. When mixed together with the scaffold proteins with RIAD, MenD−RIDD failed to be incorporated in the phase-separated condensates. Instead, adding this protein to the phase condensate caused disassembly of the condensate, evidenced by less condensate formation and higher ratio of scaffold proteins in the solution phase than the protein-phase condensate (Figure S3A). One possible reason for this phenomenon is that MenD−RIDD has certain surface property making it incompatible to the phase, or the introduction of strong peptide interaction between MenD and the scaffold proteins makes MenD−RIDD repelled from the RIAD-tagged condensates, which was also observed in recent reports on other phase-separated condensates.[27,34] Hence, among the three RIDD-tagged enzymes, only MenH−RIDD can be incorporated and enriched within the RIAD-tagged protein condensate driven by specific peptide−

https://dx.doi.org/10.1021/acs.biomac.0c00321
Biomacromolecules 2020, 21, 2391−2399

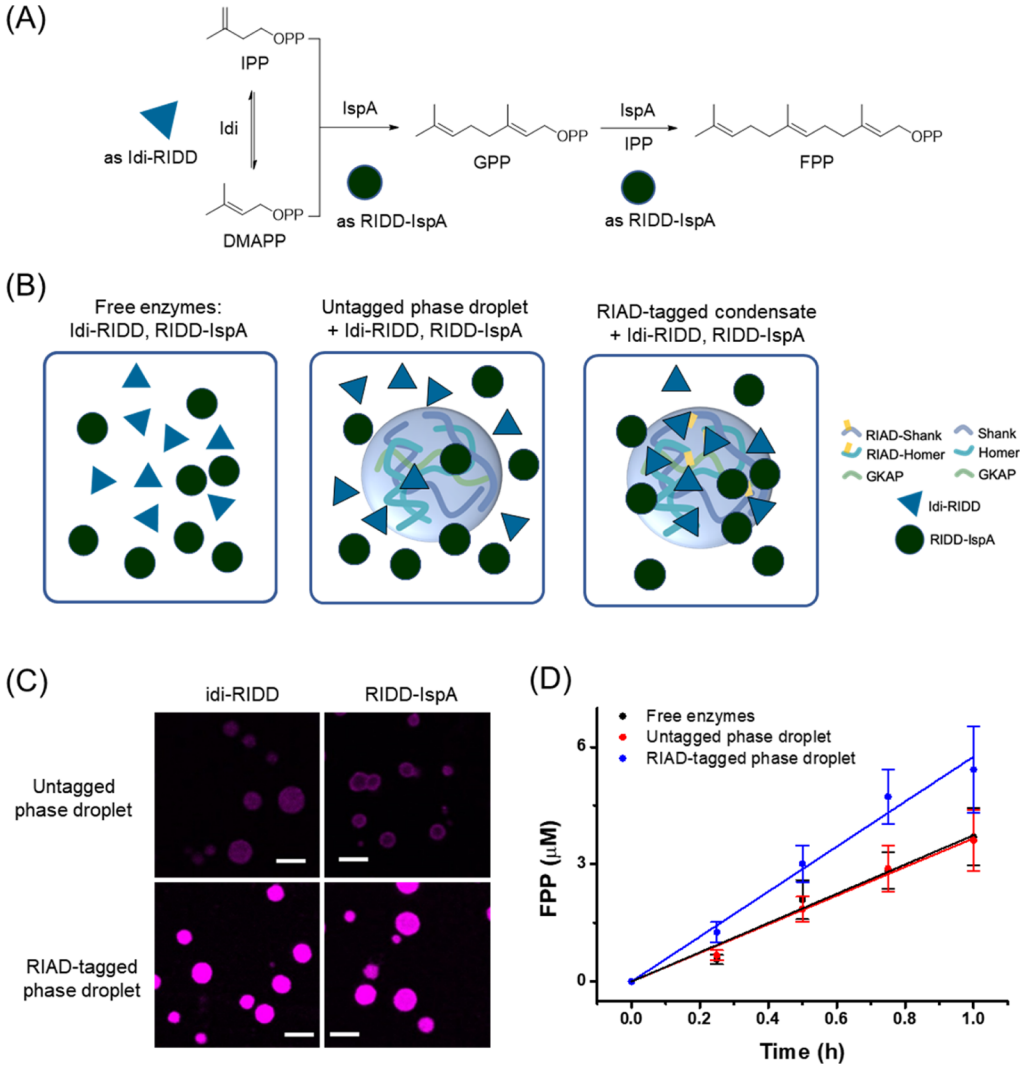

Figure 5. Assembly of terpene biosynthetic enzymes within the protein condensate promotes catalysis. (A) Idi and IspA enzyme, and reactions they catalyzed. (B) Schematic illustration of thee three multienzyme systems. (C) Confocal images of Cy5-labeled enzymes, showing the enzyme concentration differences inside and outside of the protein condensates. Scale bar: 5 μm. Protein scaffolds, 5 μM; idi-RIDD or RIDD-IspA, 0.5 μM with 10% labeled with Cy5. (D) Quantification of the initial rate of FPP production for comparison of the three systems.

peptide interaction (Figures 4D and S3B). Moreover, MenF, MenD, and MenH−RIDD can be spontaneously assembled in the untagged protein condensate formed by Shank, Homer, and GKAP. Without the assistance of a specific peptide−peptide interaction, spontaneous, "low-level" enrichment in the untagged protein condensate was observed using fluorescently labeled individual enzymes (Figures 4C and S3C). This result then allowed us to establish three multienzyme biosynthetic systems (Figure 4B).

The comparison of the three enzymatic systems revealed that MenF/MenD/MenH−RIDD in untagged condensates showed a similar catalytic production rate (k_{app} of 6.31 ± 0.26 μM SHCHC/min) as MenF/MenD/MenH−RIDD in RIAD-tagged condensates (6.80 ± 0.23 μM SHCHC/min), 70% or 83% higher than the free MenF/MenD/MenH−RIDD system (3.72 ± 0.21 μM SHCHC/min), respectively (Figure 4E). It surprised us that the two assembled systems showed similar catalytic efficiency without statistical significance ($P < 0.05$, Welch's t-test, Figure S4A), although the enrichment of MenH−RIDD in tagged or untagged systems is vastly different. One possible explanation may be that MenD is a rate-limiting enzyme, whereas MenH is a fast reaction, comparing the k_{cat} and K_m of the three enzymes.[44,45,47] Therefore, a spontaneous, "low-level" enrichment of rate-limiting enzyme MenD in the protein condensates is sufficient to significantly improve the catalytic rate, whereas further enrichment of the nonrate-limiting enzyme MenH−RIDD by the strong and specific peptide−peptide interaction did not further increase the catalytic rate.

Terpene Biosynthetic Enzymes in the Protein Condensate. Last, we examined the assembly of another cascade biosynthetic system in the protein condensate. A critical step in terpene biosynthesis is the conversion of the five-carbon units IPP and dimethylallyl pyrophosphate (DMAPP) to monoterpene geranyl pyrophosphate (GPP) and sesquiterpene FPP as the first dedicated, rate-limiting step toward terpene biosynthesis.[50] IPP and DMAPP are the products of the mevalonate (MVA) pathway or the methylerythritol 4-phosphate (MEP) pathway.[51] An *Escherichia coli* enzyme, isopentenyl-diphosphate delta-isomerase (Idi), is often used to catalyze the equilibrium between IPP and DMAPP,[52] and a farnesyl diphosphate synthase (IspA) is

https://dx.doi.org/10.1021/acs.biomac.0c00321
Biomacromolecules 2020, 21, 2391−2399

responsible for the condensation of IPP and DMAPP to give GPP and FPP (Figure 5A).[53] We, then, cloned and expressed Idi-RIDD and RIDD-IspA with RIDD fused to the C-terminus of Idi and N-terminus of IspA to avoid disturbance to the enzymatic function. Three multienzyme catalytic systems were then constructed (Figure 5B). Idi-RIDD and RIDD-IspA can both be strongly enriched by the RIAD-RIDD interaction (Figure 5C). The concentration of Idi-RIDD and RIDD-IspA inside the condensate was 56-fold and 43-fold higher than added concentration, estimated by Cy5 fluorescence (Figure S5). A comparison of the catalytic activity of the three systems showed that the Idi-RIDD/RIDD-IspA in RIAD-tagged condensates produced 5.67 ± 0.22 μM FPP/h in the initial catalytic stage, 54% or 51% faster than Idi-RIDD/RIDD-IspA in untagged condensates (3.68 ± 0.08 μM FPP/h) or free enzymes (3.76 ± 0.11 μM FPP/h) (Figure 5D). The results indicated that the coassembly and enrichment of both Idi-RIDD and RIDD-IspA by the peptide−peptide interaction could increase the catalytic rate of this cascade enzyme system.

CONCLUSIONS

Assembling enzymes within the protein phase-separated condensates allows the exploration of the interplay of phase separation and multienzyme catalysis. Here, we engineered PSD-derived component proteins as the scaffold to form the synthetic phase-separated protein condensate that is capable of assembling enzymes through a specific, high-affinity peptide−peptide interaction. Three sets of proteins, including fluorescent proteins, and two sets of sequential enzymes were assembled with the condensate, manifesting the versatility of the scaffold system. Most RIDD-tagged proteins, we expressed, can be enriched within the condensates with more than 50-fold enrichment except MenD−RIDD. Second, the fluorescent proteins assembled within the condensate showed a wide range of FRET signal, suggesting the heterogeneity of the protein distribution in the protein condensate. This work presents examples from the perspective of multienzyme catalysis that assembling enzymes with phase-separating proteins significantly improves catalytic efficiency than that of free floating enzymes—a benefit that might be harnessed from early prebiotic world all the way to modern cells. Altogether, this work presents a new approach of improving catalysis by physical assembly and provides a hint for the formation and benefit of membrane-less organelles.

ASSOCIATED CONTENT

Supporting Information

The Supporting Information is available free of charge at https://pubs.acs.org/doi/10.1021/acs.biomac.0c00321.

Detailed experimental procedures; list of protein sequences; assembly of EGFP in the protein phase condensate; exchange of fluorescent proteins between CFP and YFP condensates; fluorescent signal distribution in CFP only and CFP + YFP condensates by boxplots; centrifugation/SDS−PAGE analysis showing the protein distributions of the menaquinone biosynthetic enzymes in the protein condensate; catalytic property of the menaquinone biosynthetic enzyme condensates; and estimating concentration of terpene biosynthetic enzymes inside the protein condensate (PDF)

AUTHOR INFORMATION

Corresponding Author

Jiang Xia − *Department of Chemistry, School of Life Sciences and Center for Cell & Developmental Biology, School of Life Sciences, The Chinese University of Hong Kong, Shatin, Hong Kong SAR, China;* orcid.org/0000-0001-8112-7625; Phone: (852) 3943 6165; Email: jiangxia@cuhk.edu.hk; Fax: (852) 2603 5057

Authors

Miao Liu − *Department of Chemistry, School of Life Sciences, The Chinese University of Hong Kong, Shatin, Hong Kong SAR, China*

Sicong He − *Department of Electronic and Computer Engineering, Center of Systems Biology and Human Health, School of Science and Institute for Advanced Study, Hong Kong University of Science and Technology, Kowloon, Hong Kong SAR, China*

Lixin Cheng − *Department of Critical Care Medicine, Shenzhen People's Hospital, First Affiliated Hospital of Southern University of Science and Technology, Shenzhen 518000, China*

Jianan Qu − *Department of Electronic and Computer Engineering, Center of Systems Biology and Human Health, School of Science and Institute for Advanced Study, Hong Kong University of Science and Technology, Kowloon, Hong Kong SAR, China;* orcid.org/0000-0002-6809-0087

Complete contact information is available at: https://pubs.acs.org/10.1021/acs.biomac.0c00321

Author Contributions

J.X. conceived the project, designed experiments and wrote the manuscript. M.L. and S.H. carried out the experiments. L.C. and J.Q. helped analyze the data.

Notes

The authors declare no competing financial interest.

ACKNOWLEDGMENTS

The authors acknowledge Prof. Mingjie Zhang at the Hong Kong University of Science and Technology for providing the constructs of GKAP, Shank, and Homer. This work was partially funded by grants by University Grants Committee of Hong Kong (GRF grants 14304915, 14321116, 14306317, 14307218, and AoE/M-09/12) and Food and Health Bureau (HMRF 15140052).

ABBREVIATIONS

PSD, postsynaptic density; SHCHC, 2-succinyl-6-hydroxy-2,4-cyclohexadiene-1-carboxylate; FPP, farnesyl pyrophosphate; LLPS, liquid−liquid phase separations; FRET, fluorescence resonance energy transfer; Cy5, Cyanine5

REFERENCES

(1) Fox, S. W. The Evolutionary Significance of Phase-Separated Microsystems. *Orig. Life* **1976**, *7*, 49−68.

(2) Poudyal, R. R.; Pir Cakmak, F.; Keating, C. D.; Bevilacqua, P. C. Physical principles and extant biology reveal roles for RNA-containing membraneless compartments in origins of life chemistry. *Biochemistry* **2018**, *57*, 2509−2519.

(3) Schreiber, A.; Huber, M. C.; Schiller, S. M. Prebiotic Protocell Model Based on Dynamic Protein Membranes Accommodating Anabolic Reactions. *Langmuir* **2019**, *35*, 9593−9610.

(4) Shin, Y.; Brangwynne, C. P. Liquid phase condensation in cell physiology and disease. *Science* **2017**, *357*, No. eaaf4382.

(5) Banani, S. F.; Lee, H. O.; Hyman, A. A.; Rosen, M. K. Biomolecular condensates: organizers of cellular biochemistry. *Nat. Rev. Mol. Cell Biol.* **2017**, *18*, 285−298.
(6) Boeynaems, S.; Alberti, S.; Fawzi, N. L.; Mittag, T.; Polymenidou, M.; Rousseau, F.; Schymkowitz, J.; Shorter, J.; Wolozin, B.; Van Den Bosch, L.; Tompa, P.; Fuxreiter, M. Protein Phase Separation: A New Phase in Cell Biology. *Trends Cell Biol.* **2018**, *28*, 420−435.
(7) Alberti, S.; Gladfelter, A.; Mittag, T. Considerations and Challenges in Studying Liquid-Liquid Phase Separation and Biomolecular Condensates. *Cell* **2019**, *176*, 419−434.
(8) Bracha, D.; Walls, M. T.; Brangwynne, C. P. Probing and engineering liquid-phase organelles. *Nat. Biotechnol.* **2019**, *37*, 1435−1445.
(9) Sabari, B. R.; Dall'Agnese, A.; Boija, A.; Klein, I. A.; Coffey, E. L.; Shrinivas, K.; Abraham, B. J.; Hannett, N. M.; Zamudio, A. V.; Manteiga, J. C.; Li, C. H.; Guo, Y. E.; Day, D. S.; Schuijers, J.; Vasile, E.; Malik, S.; Hnisz, D.; Lee, T. I.; Cisse, I. I.; Roeder, R. G.; Sharp, P. A.; Chakraborty, A. K.; Young, R. A. Coactivator condensation at super-enhancers links phase separation and gene control. *Science* **2018**, *361*, No. eaar3958.
(10) Larson, A. G.; Elnatan, D.; Keenen, M. M.; Trnka, M. J.; Johnston, J. B.; Burlingame, A. L.; Agard, D. A.; Redding, S.; Narlikar, G. J. Liquid condensate formation by HP1α suggests a role for phase separation in heterochromatin. *Nature* **2017**, *547*, 236−240.
(11) Strom, A. R.; Emelyanov, A. V.; Mir, M.; Fyodorov, D. V.; Darzacq, X.; Karpen, G. H. Phase separation drives heterochromatin domain formation. *Nature* **2017**, *547*, 241−245.
(12) Jiang, H.; Wang, S.; Huang, Y.; He, X.; Cui, H.; Zhu, X.; Zheng, Y. Phase transition of spindle-associated protein regulate spindle apparatus assembly. *Cell* **2015**, *163*, 108−122.
(13) Shan, Z.; Tu, Y.; Yang, Y.; Liu, Z.; Zeng, M.; Xu, H.; Long, J.; Zhang, M.; Cai, Y.; Wen, W. Basal condensation of Numb and Pon complex via phase transition during Drosophila neuroblast asymmetric division. *Nat. Commun.* **2018**, *9*, 737.
(14) Sun, D.; Wu, R.; Zheng, J.; Li, P.; Yu, L. Polyubiquitin chain-induced p62 phase separation drives autophagic cargo segregation. *Cell Res.* **2018**, *28*, 405−415.
(15) Zhang, G.; Wang, Z.; Du, Z.; Zhang, H. mTOR Regulates Phase Separation of PGL Granules to Modulate Their Autophagic Degradation. *Cell* **2018**, *174*, 1492−1506.
(16) Du, M.; Chen, Z. J. DNA-induced liquid phase condensation of cGAS activates innate immune signaling. *Science* **2018**, *361*, 704−709.
(17) O'Connell, J. D.; Zhao, A.; Ellington, A. D.; Marcotte, E. M. Dynamic reorganization of metabolic enzymes into intracellular bodies. *Annu. Rev. Cell Dev. Biol.* **2012**, *28*, 89−111.
(18) Prouteau, M.; Loewith, R. Regulation of Cellular Metabolism through Phase Separation of Enzymes. *Biomolecules* **2018**, *8*, 160.
(19) Noree, C.; Monfort, E.; Shiau, A. K.; Wilhelm, J. E. Common regulatory control of CTP synthase enzyme activity and filament formation. *Mol. Biol. Cell* **2014**, *25*, 2282−2290.
(20) Pedley, A. M.; Benkovic, S. J. A New View into the Regulation of Purine Metabolism: The Purinosome. *Trends Biochem. Sci.* **2017**, *42*, 141−154.
(21) Zhao, E. M.; Suek, N.; Wilson, M. Z.; Dine, E.; Pannucci, N. L.; Gitai, Z.; Avalos, J. L.; Toettcher, J. E. Light-based control of metabolic flux through assembly of synthetic organelles. *Nat. Chem. Biol.* **2019**, *15*, 589−597.
(22) Castellana, M.; Wilson, M. Z.; Xu, Y.; Joshi, P.; Cristea, I. M.; Rabinowitz, J. D.; Gitai, Z.; Wingreen, N. S. Enzyme clustering accelerates processing of intermediates through metabolic channeling. *Nat. Biotechnol.* **2014**, *32*, 1011−1018.
(23) Crowe, C. D.; Keating, C. D. Liquid−liquid phase separation in artificial cells. *Interface Focus* **2018**, *8*, 20180032.
(24) Strulson, C. A.; Molden, R. C.; Keating, C. D.; Bevilacqua, P. C. RNA catalysis through compartmentalization. *Nat. Chem.* **2012**, *4*, 941−946.
(25) Shin, Y.; Berry, J.; Pannucci, N.; Haataja, M. P.; Toettcher, J. E.; Brangwynne, C. P. Spatiotemporal Control of Intracellular Phase Transitions Using Light-Activated optoCondensates. *Cell* **2017**, *168*, 159−171.
(26) Banani, S. F.; Rice, A. M.; Peeples, W. B.; Lin, Y.; Jain, S.; Parker, R.; Rosen, M. K. Compositional Control of Phase-Separated Cellular Bodies. *Cell* **2016**, *166*, 651−663.
(27) Schuster, B. S.; Reed, E. H.; Parthasarathy, R.; Jahnke, C. N.; Caldwell, R. M.; Bermudez, J. G.; Ramage, H.; Good, M. C.; Hammer, D. A. Controllable protein phase separation and modular recruitment to form responsive membraneless organelles. *Nat. Commun.* **2018**, *9*, 2985.
(28) Wong, W.; Scott, J. D. AKAP signalling complexes: focal points in space and time. *Nat. Rev. Mol. Cell Biol.* **2004**, *5*, 959−970.
(29) Sarma, G. N.; Kinderman, F. S.; Kim, C.; von Daake, S.; Chen, L.; Wang, B.-C.; Taylor, S. S. Structure of D-AKAP2:PKA RI complex: insights into AKAP specificity and selectivity. *Structure* **2010**, *18*, 155−166.
(30) Kang, W.; Ma, T.; Liu, M.; Qu, J.; Liu, Z.; Zhang, H.; Shi, B.; Fu, S.; Ma, J.; Lai, L. T. F.; He, S.; Qu, J.; Au, S. W.; Kang, B. H.; Lau, W. C. Y.; Deng, Z.; Xia, J.; Liu, T. Modular enzyme assembly for enhanced cascade biocatalysis and metabolic flux. *Nat. Commun.* **2019**, *10*, 4248.
(31) Carlson, C. R.; Lygren, B.; Berge, T.; Hoshi, N.; Wong, W.; Taskén, K.; Scott, J. D. Delineation of type I protein kinase A-selective signaling events using an RI anchoring disruptor. *J. Biol. Chem.* **2006**, *281*, 21535−21545.
(32) Sheng, M.; Kim, E. The postsynaptic organization of synapses. *Cold Spring Harbor Perspect. Biol.* **2011**, *3*, a005678.
(33) Zeng, M.; Shang, Y.; Araki, Y.; Guo, T.; Huganir, R. L.; Zhang, M. Phase Transition in Postsynaptic Densities Underlies Formation of Synaptic Complexes and Synaptic Plasticity. *Cell* **2016**, *166*, 1163−1175.
(34) Zeng, M.; Chen, X.; Guan, D.; Xu, J.; Wu, H.; Tong, P.; Zhang, M. Reconstituted Postsynaptic Density as a Molecular Platform for Understanding Synapse Formation and Plasticity. *Cell* **2018**, *174*, 1172−1187.
(35) Zeng, M.; Díaz-Alonso, J.; Ye, F.; Chen, X.; Xu, J.; Ji, Z.; Nicoll, R. A.; Zhang, M. Phase Separation-Mediated TARP/MAGUK Complex Condensation and AMPA Receptor Synaptic Transmission. *Neuron* **2019**, *104*, 529−543.
(36) Guimerà, R.; Nunes Amaral, L. A. Functional cartography of complex metabolic networks. *Nature* **2005**, *433*, 895−900.
(37) Cheng, L.; Fan, K.; Huang, Y.; Wang, D.; Leung, K.-S. Full characterization of localization diversity in the human protein interactome. *J. Proteome Res.* **2017**, *16*, 3019−3029.
(38) Cheng, L.; Leung, K.-S. Identification and characterization of moonlighting long non-coding RNAs based on RNA and protein interactome. *Bioinformatics* **2018**, *34*, 3519−3528.
(39) Cheng, Y.; Patel, D. J. An efficient system for small protein expression and refolding. *Biochem. Biophys. Res. Commun.* **2004**, *317*, 401−405.
(40) Goedhart, J.; van Weeren, L.; Hink, M. A.; Vischer, N. O. E.; Jalink, K.; Gadella, T. W. J., Jr. Bright cyan fluorescent protein variants identified by fluorescence lifetime screening. *Nat. Methods* **2010**, *7*, 137−139.
(41) Nagai, T.; Ibata, K.; Park, E. S.; Kubota, M.; Mikoshiba, K.; Miyawaki, A. A variant of yellow fluorescent protein with fast and efficient maturation for cell-biological applications. *Nat. Biotechnol.* **2002**, *20*, 87−90.
(42) Kurosu, M.; Begari, E. Vitamin K2 in electron transport system: are enzymes involved in vitamin K2 biosynthesis promising drug targets? *Molecules* **2010**, *15*, 1531−1553.
(43) Meganathan, R.; Kwon, O. Biosynthesis of Menaquinone (Vitamin K2) and Ubiquinone (Coenzyme Q). *EcoSal Plus* **2009**, *3*, 173−218.
(44) Daruwala, R.; Bhattacharyya, D. K.; Kwon, O.; Meganathan, R. Menaquinone (vitamin K2) biosynthesis: overexpression, purification, and characterization of a new isochorismate synthase from Escherichia coli. *J. Bacteriol.* **1997**, *179*, 3133−3138.

https://dx.doi.org/10.1021/acs.biomac.0c00321
Biomacromolecules 2020, 21, 2391−2399

(45) Jiang, M.; Cao, Y.; Guo, Z.-F.; Chen, M.; Chen, X.; Guo, Z. Menaquinone biosynthesis in Escherichia coli: Identification of 2-succinyl-5-enolpyruvyl-6-hydroxy-3-cyclohexene-1-carboxylate (SEPHCHC) as a novel intermediate and re-evaluation of MenD activity. *Biochemistry* **2007**, *46*, 10979−10989.
(46) Jiang, M.; Chen, M.; Cao, Y.; Yang, Y.; Sze, K. H.; Chen, X.; Guo, Z. Determination of the stereochemistry of 2-succinyl-5-enolpyruvyl-6-hydroxy-3-cyclohexene-1-carboxylic acid, a key intermediate in menaquinone biosynthesis. *Org. Lett.* **2007**, *9*, 4765−4767.
(47) Jiang, M.; Chen, X.; Guo, Z.-F.; Cao, Y.; Chen, M.; Guo, Z. Identification and characterization of (1R,6R)-2-succinyl-6-hydroxy-2,4-cyclohexadiene-1-carboxylate synthase in the menaquinone biosynthesis of Escherichia coli. *Biochemistry* **2008**, *47*, 3426−3434.
(48) Liu, Z.; Cao, S.; Liu, M.; Kang, W.; Xia, J. Self-Assembled Multienzyme Nanostructures on Synthetic Protein Scaffolds. *ACS Nano* **2019**, *13*, 11343−11352.
(49) Kang, W.; Liu, J.; Wang, J.; Nie, Y.; Guo, Z.; Xia, J. Cascade biocatalysis by multienzyme-nanoparticle assemblies. *Bioconjugate Chem.* **2014**, *25*, 1387−1394.
(50) Zhu, F.; Zhong, X.; Hu, M.; Lu, L.; Deng, Z.; Liu, T. In vitro reconstitution of mevalonate pathway and targeted engineering of farnesene overproduction in Escherichia coli. *Biotechnol. Bioeng.* **2014**, *111*, 1396−1405.
(51) Paniagua-Michel, J.; Olmos-Soto, J.; Ruiz, M. A. Pathways of carotenoid biosynthesis in bacteria and microalgae. *Methods Mol. Biol.* **2012**, *892*, 1−12.
(52) Hahn, F. M.; Hurlburt, A. P.; Poulter, C. D. Escherichia coli open reading frame 696 is idi, a nonessential gene encoding isopentenyl diphosphate isomerase. *J. Bacteriol.* **1999**, *181*, 4499−4504.
(53) Hosfield, D. J.; Zhang, Y.; Dougan, D. R.; Broun, A.; Tari, L. W.; Swanson, R. V.; Finn, J. Structural basis for bisphosphonate-mediated inhibition of isoprenoid biosynthesis. *J. Biol. Chem.* **2004**, *279*, 8526−8529.

https://dx.doi.org/10.1021/acs.biomac.0c00321
Biomacromolecules 2020, 21, 2391−2399